DOI: 10.1002/cnma.201500048

High-Index Surfaces

High-Indexed Pt_3Fe Nanocatalysts and Their Enhanced Catalytic Performance in Dual Organic Reactions

Chenyu Wang,[a] Cuikun Lin,[b] Bo Zhao,[b] Lihua Zhang,[c] Amar Kumbhar,[d] Guangyin Fan,[a, e] Kai Sun,[f] Jun Zhang,[g] Shuang Chen,[g] and Jiye Fang*[a]

Abstract: The synthesis of noble metal nanocrystals terminated with high-index facets has received increasing attention due to the remarkable improvement in their catalytic performance. Introducing a transition metal to noble metals (bimetallic nanocrystals) could result in a reduced cost and potentially improve properties. Keeping in mind both of these advantages, we have developed a new synthetic approach to fabricate size-controlled Pt_3Fe concave nanocubes using a high-temperature organic solution system containing oleylamine and oleic acid. It further demonstrates that the particle size and concavity could be controlled by a number of parameters such as the ratio of oleylamine and oleic acid, the physicochemical properties of the metal carbonyl, the metal valence in the precursor, and the ratio of metal precursors. Catalytic tests show that the high-index-surface-terminated $\approx$12 nm Pt_3Fe concave nanocubes exhibit superior performance in both the hydrogenation of styrene and reduction of 4-nitrophenol in comparison with their counterparts.

Introduction

With the advent of emerging nanotechnology, catalysts have been developing exponentially in the past decade. Among various classes of catalysts, noble metal nanocrystals (NCs) are of tremendous interest primarily due to their fascinating performances in a series of catalytic transformations including hydrogenation, coupling, and hydrocracking reactions.[1] However, the preciousness and limited reservoir of noble metals especially platinum (Pt), an extremely scarce element in the earth's crust, severely hinder their commercialization. Extensive efforts have therefore been exerted to fully exploit their potential for catalysis. Since a heterogeneous catalytic process is closely associated with the surface structure of the catalyst, the catalytic performance could be further improved by altering the atomic arrangement on the exposed surfaces of the catalyst through tailoring their particle shape.[2] As is well known, atoms located at steps, ledges, and kinks of a crystal could act as catalytically active sites,[3] and it is significant to rationally design and prepare shape-controlled nanocatalysts with a high density of low-coordinated atoms. Accordingly, customization of noble metal NCs with high-index crystallographic facets (HIFs) has been explored as an effective mean to achieve this goal. On the other hand, it has been demonstrated that catalytic performance could be enhanced by alloying a noble metal with another to form alloy nanocatalysts.[4] Previous studies further indicate that incorporation of a less expensive transition metal M (such as Cu, or Co, or Ni, or Fe) into a noble metal NC will not only reduce the use of scarce noble metal but also improve their electrocatalytic[5] and organic catalytic[6] performance, benefiting from the modified surface electronic

[a] Dr. C. Wang, Dr. G. Fan, Prof. J. Fang
Department of Chemistry
State University of New York at Binghamton
Binghamton, New York 13902 (USA)
E-mail: jfang@binghamton.edu

[b] Dr. C. Lin, Dr. B. Zhao
Department of Chemistry
University of South Dakota
Vermillion, South Dakota 57069 (USA)

[c] Dr. L. Zhang
Center for Functional Nanomaterials
Brookhaven National Laboratory
Upton, New York 11973 (USA)

[d] Dr. A. Kumbhar
Chapel Hill Analytical and Nanofabrication Laboratory
University of North Carolina at Chapel Hill
Chapel Hill, North Carolina 27599 (USA)

[e] Dr. G. Fan
Chemical Synthesis and Pollution Control
Key Laboratory of Sichuan Province
College of Chemistry and Chemical Industry
China West Normal University
Nanchong, Sichuan 637009 (China)

[f] Dr. K. Sun
Department of Materials Science and Engineering
University of Michigan
Ann Arbor, Michigan 48109 (USA)

[g] Dr. J. Zhang, Dr. S. Chen
College of Chemical Engineering
China University of Petroleum
Qingdao, Shandong 266580 (China)

Supporting information for this article is available on the WWW under http://dx.doi.org/10.1002/cnma.201500048.

structure.[7] However, little work of applying HIF-terminated noble-transition bimetallic NCs as catalysts to traditional organic reactions has been reported.

Concave nanostructures, being a prototype of high-index-faceted NCs, are distinguished by their branched morphologies and ease of preparation in the solution phase governed by diffusion.[8] Although Pt–Fe concave nanocubes (CNCbs) were prepared recently,[9] their size and concavity are not tunable and the governing parameters leading to the concave structure have not been well elucidated. Moreover, their catalytic behaviors towards a general organic reaction have not been systematically investigated with a selection of appropriate model reactions. In this work, we are dedicated to the preparation of ≈10 nm Pt_3Fe CNCbs using a different synthetic strategy and we demonstrate their enhanced catalytic reactivity in dual-model organic reactions: hydrogenation of styrene and reduction of 4-nitrophenol (4-NP).

Results and Discussion

Structure and composition analysis

In a typical synthesis, metal precursors $Pt(acac)_2$ and $Fe(acac)_3$ (acac: acetylacetonate) were co-reduced into Pt_3Fe CNCbs in dark-brown colloidal suspensions by tungsten hexacarbonyl [$W(CO)_6$] in the presence of oleylamine (OAm) and oleic acid (OA) at 240 °C for 40–50 min. The detailed synthesis procedure can be found in the Experimental Section. Transmission electron microscopy (TEM) images of the as-prepared Pt_3Fe NCs indicate a selective growth of highly uniform cubic nanostructures with curved surfaces and good uniformity (Figure 1a). With a focus on an individual Pt_3Fe NC (Figure 1c), it appears that the near-edge parts have lower contrast in comparison with the central portion, suggesting that the NC surface was partially excavated towards the centre to form a concave nanostructure as illustrated in Figure 1b. On the basis of the TEM image shown in Figure 1a, the average side length was determined as 12.1 ± 1.0 nm (hereafter, referred as 10 nm Pt_3Fe CNCbs). A high-resolution TEM (HRTEM) image (Figure 1c) was taken of a selected Pt_3Fe CNCb with a projection direction along [001]. The projection orientation was confirmed by its corresponding fast Fourier transform (FFT) pattern (Figure 1d). From the HRTEM image, the measured average *d* spacing of 1.94 Å is consistent with that for Pt_3Fe {200}.[10] Angles between each of the actual surface planes and (100) facet of an ideal cube were measured as 24°, 19°, 22°, and 20° as marked in Figure 1c, confirming that the generated concave surfaces are HIFs. As shown in Figure 1e (a selected region from Figure 1c), stepped surface consisting of {100} terraces and {110} steps can be readily observed. In particular, surfaces of a CNCb are mixtures of several {*hk*0} facets (Figure 1f) rather than sub-facets with a certain group of Miller indices.

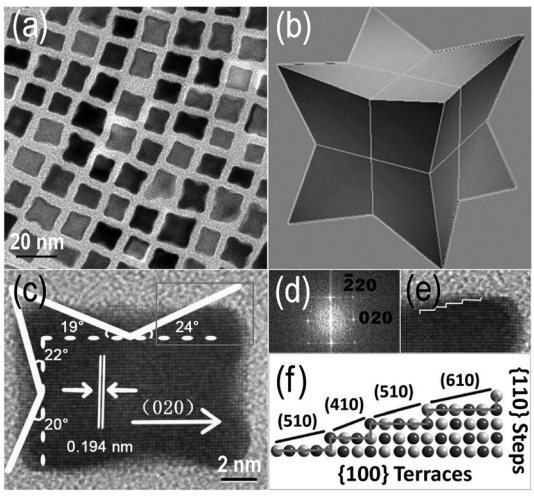

Figure 1. Images of ≈10 nm Pt_3Fe CNCbs. (a) TEM image of the as-prepared Pt_3Fe CNCbs; (b) 3D perspective illustration model of a concave cube; (c) HRTEM of a single Pt_3Fe CNCb; (d) fast Fourier transform pattern of the CNCb shown in (c); (e) a stepped surface highlighted from the HRTEM image; (f) scheme of the stepped surface composed of a mixture of high-index facets with {100} terraces and {110} steps.

The chemical composition of the CNCbs was determined using inductively coupled plasma-optical emission spectrometry (ICP-OES). Analysis indicates that the Pt/Fe molar ratio was ≈3:1, which is in a good agreement with the preceding estimation from the lattice spacing. As presented in Figure 2a, the

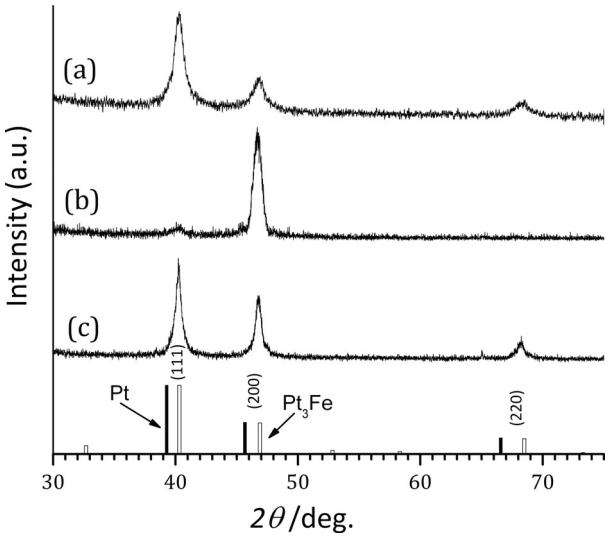

Figure 2. XRD patterns of Pt_3Fe CNCbs: (a) as-prepared Pt_3Fe CNCbs randomly deposited on a PANalytical zero-background Si sample holder; (b) the same sample assembled on a surface-polished 25 mm Si <100> wafer; (c) the Pt_3Fe CNCbs in size of 20 nm prepared in the presence of $Cr(CO)_6$ and randomly deposited on a PANalytical zero-background Si sample holder. The patterns shown at the bottom are from standard Pt ICDD PDF cards (black: Pt 88-2343; White: Pt_3Fe 89-2050).

X-ray diffraction (XRD) pattern of the Pt_3Fe CNCbs confirms that the as-synthesized NCs possess a highly crystalline face-centered cubic (*fcc*) phase. The slight rightward peak-shift in such a pattern in comparison with the standard Pt peaks is due to shrinkage of the lattices, demonstrating the formation of Pt–Fe alloy NCs. A greatly enhanced (200) peak (Figure 2b) could be detected when these CNCbs were carefully deposited on a surface-polished Si wafer, indicating that these Pt_3Fe

CNCbs align perfectly flat on the surface of the substrates with (100) texture. Apparently, no diffraction signal of a single metal is detectable from these patterns.

Formation conditions and mechanism

The HIF-containing CNCbs are metastable in a solution phase and therefore tend to thermodynamically transform into low-index-faceted analogues.[11] The first prerequisite for achieving such a nanostructure is a fast growth rate under a kinetic control, which is correlated with selective binding of surfactants, the reaction/diffusion rate, and the solubility of precursors.[2b] In view of this, several conditions such as the volume ratio of OAm/OA, capability of metal carbonyl, and selection of the metal should be rigorously examined and optimized, aiming to an understanding of the formation mechanism.

(1) Volume ratio of OAm/OA

In recognition of the capping effect of OAm and OA, the OAm/OA volume ratio used for the syntheses was varied from 10:1 to 4:1 and selected resultant morphologies are shown in Figure 3a and 3b. We have also explored a ratio of higher than 10:1, attaining NCs in two classes of sizes. With decreasing the OAm/OA volume ratio from 10:1 to 4:1, it can be observed that the concave feature transitions to flat-like surfaces. It is therefore inferred that a high OAm/OA ratio might favor the formation of HIFs and restrict the atomic addition to concave sites, thereby preserving the HIFs and concave structure. To further identify the roles played by the OAm/OA in the formation of NCs, it is necessary to monitor their growth process at a high OAm/OA ratio (10:1). Figure S1 in the Supporting Information shows the morphologies of NCs that were collected at different times from the reaction system. As shown in Figure S1a, minuscule NCs can be identified as nuclei in the foremost stage. Then, they rapidly transform to highly branched and faceted NCs as intermediates of larger size compared to that of the ultimate Pt_3Fe CNCbs (Figure S1b). By taking a glance at the image of higher magnification (inset of Figure S1b), these intermediates of Pt_3Fe CNCbs were essentially constituted of interconnected arms, which is fairly similar to the multioctahedral Pt NCs synthesized in the presence of a trace amount of Fe^{3+} ions.[12] These random multipods gradually developed into NCs with more uniform size and well-defined concave cubic profile (Figure S1c and d), indicating that formation of multipods is an essential pathway between the nucleating seeds and eventual CNCbs at a high OAm/OA ratio, and the overall reduction kinetics are pivotal in the shape control in this case.

Similar evolution intermediates were also observed in the Pt–Cu system[13] although the synthesis approach is not exactly commensurate with this one. The structure of hydrocarbon chain was also examined by replacing OAm or OA in 10:1 OAm-OA with octylamine or lauric acid, respectively. As illustrated in Figure S2, the harvested small NCs are neither cubes nor CNCbs in shape.

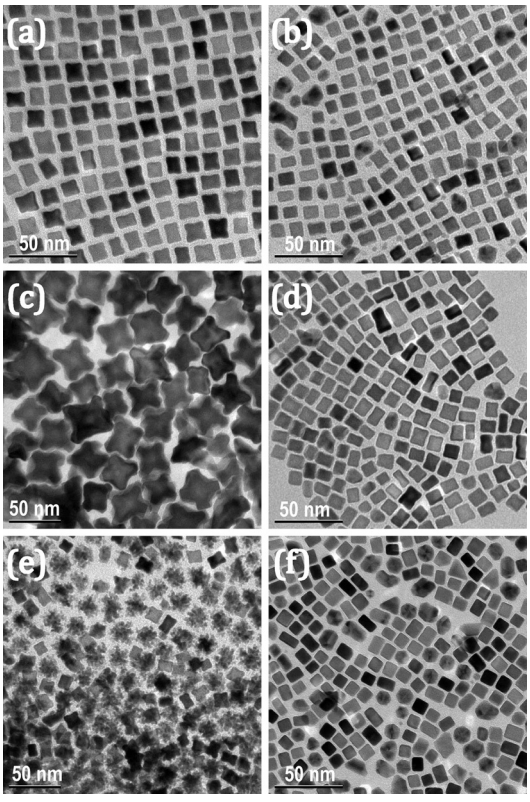

Figure 3. TEM images of Pt–Fe NCs grown for 40 min under the typical synthetic conditions (see Experimental Section), except for the following variation in each case: (a) typical conditions (the volume ratio of OAm/OA was 10:1); (b) the volume ratio of OAm/OA was 4:1; (c) $W(CO)_6$ was replaced with $Cr(CO)_6$; (d) $Fe(acac)_3$ was replaced with $FeCl_2{\cdot}4H_2O$ as the precursors; (e) the amount of $Pt(acac)_2$ as the precursor was increased; (f) Fe precursors were absent.

(2) Capability of metal carbonyl

As discussed previously,[14] the involved $W(CO)_6$ could act with dual roles: providing both metallic W as a reducing agent and CO to control the shape of seeds and to help reduce high valence metal(s) added. Since the reaction kinetics could be strongly associated with the reducing capability, W in the metal carbonyls was studied by replacing with Cr using the typical synthesis recipe. The employment of chromium hexacarbonyl [$Cr(CO)_6$] could still generate Pt_3Fe CNCbs (Figure 2c) but the average size is larger ($\approx$20 nm, Figure 3c). In addition, it was determined that the time to achieve CNCbs was evidently shortened, indicating that both the nucleation process and successive Ostwald ripening growth are accelerated, most likely owing to the higher concentration of metal atoms reduced by more active Cr (standard reduction potentials: $Cr^{2+} + 2e^- \rightleftharpoons Cr$, $Ep = -0.913$ V; $Cr^{3+} + 3e^- \rightleftharpoons Cr$, $Ep = -0.744$ V; $W^{3+} + 3e^- \rightleftharpoons W$, $Ep = 0.1$ V). It was generally recognized that for a kinetic-controlled reaction the growth behavior and final NC shape are dependent on a competition between the diffusion rate of atoms to the surface of NCs and the reduction rate of generating adatoms.[15] In the case of $Cr(CO)_6$, a high concentration of adatoms reduced by active Cr may quickly deposit on CNCb corners where the density of capped ligands is rela-

tively low.[16] The addition of atoms on the corners could occur almost instantly, which would not allow them migrate along the faces or edges. Consequently, large CNCbs with high degree of concavity were generated.

(3) Effect of metallic valence in precursor

It was reported that the valence states of metallic precursor could affect the shape control especially for bimetallic alloys,[17] exemplified by CuCl and $CuCl_2$ in the synthesis of Pt–Cu nanoctahedra.[5c] Likewise, it was observed in this work that the concavity of the generated Pt–Fe CNCbs was apparently weakened when $Fe(acac)_3$ was replaced with divalent $FeCl_2{\cdot}4H_2O$ while keeping other conditions identical (Figure 3d). To further elucidate valence effect, a similar synthesis was carried out at OAm/OA = 4:1. Unlike the trivalence Fe-precursors for which the products still retains some concavity, the obtained NCs were conventional cubes with flat surfaces under this condition as shown in Figure S3a. Analogously, the role of Pt^{II} precursor was investigated by replacing the original $Pt(acac)_2$ with $PtCl_4$ as the Pt source. As indicated in Figure S3b, the resultant NCs are shallowly concave, just resembling those generated by $FeCl_2{\cdot}4H_2O$ (Figure S3a). We therefore propose that presence of Fe^{II} intermediates and one-step reduction of Pt^{II} favorably tailor the Pt–Fe NCs to a CNCb profile.

(4) Effect on binary input ratio

It was observed that the quality of Pt–Fe CNCbs is also dependent on the input ratio of metallic precursors. Increase of the Pt-precursor dosage resulted in flower-like nanostructures (Figure 3e), whereas an absence of the Fe-precursor generates conventional nanocubes as the dominant products (Figure 3f). On the other hand, a decrease of the Pt-precursor dosage brought little influence on the concave shape (Figure S3c), implying a significant role of the Fe-precursor in the formation CNCbs. Notably, the OAm/OA ratio, reducing agent, and metal precursors are the paramount factors synergistically controlling the shape evolution of Pt–Fe CNCbs, as illustrated in Scheme 1.

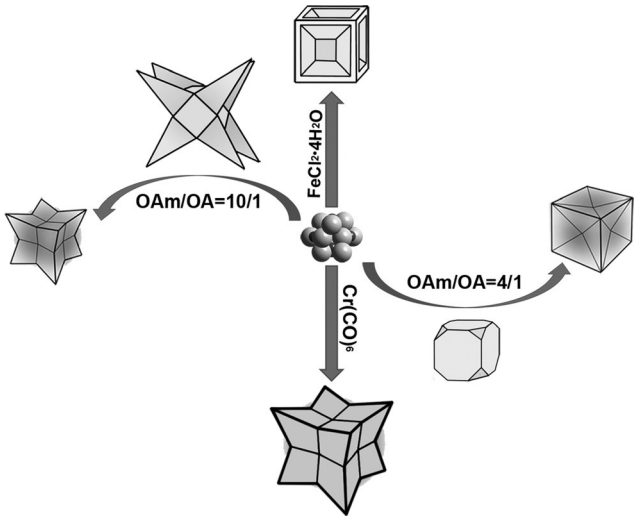

Scheme 1. An illustration of Pt–Fe NCs in different shapes synthesized under different conditions.

Catalytic performance

Catalytic hydrogenation of olefinic compounds is a popular reaction for their diverse applications in petroleum and food industries.[18] The catalytic ability of the as-synthesized Pt_3Fe CNCbs and their unique surface-dependent performance were probed within the context of a model reaction: hydrogenation of styrene. Their size, morphology and composition were confirmed by STEM (Figure S4) and ICP-OES (Table S1) results. In order to investigate the size-, structure- and composition-dependent activity, large Pt_3Fe CNCbs (≈20 nm), conventional 10 nm Pt_3Fe nanocubes, and 10 nm Pt nanocubes were also prepared and tested as references. Their TEM images observed after the catalytic tests are shown in Figure S5. The catalytic performances of these NCs were evaluated by the liquid-phase hydrogenation of styrene to ethylbenzene carried out under the same conditions (room temperature and 1 atm hydrogen atmosphere). To monitor the reaction progress, the reaction solution was sampled using an interval of every 20 min and quantitatively analyzed using a nuclear magnetic resonance spectroscope (NMR). A plot with a linear relationship observed from the conversion versus time implies a (pseudo-) zero-order kinetic dependence of styrene (Figure 4), which was common

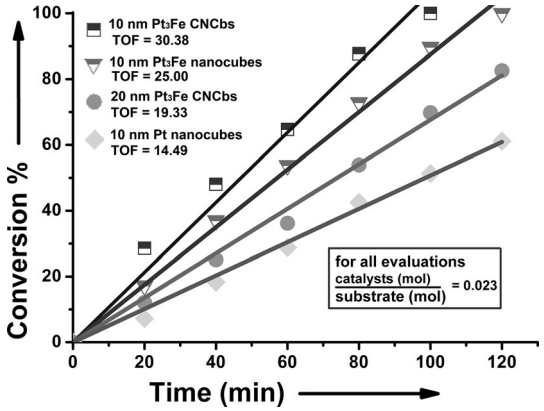

Figure 4. Conversion percentage of styrene hydrogenation as a function of reaction time. Catalysts: 10 nm Pt_3Fe CNCbs (square), 10 nm Pt_3Fe nanocubes (triangle); 20 nm Pt_3Fe CNCbs (dot) and 10 nm Pt nanocubes (diamond). Inset: TOFs of catalysts in unit of mol (products)·mol (catalysts)$^{-1}$ h^{-1}.

in the heterogeneous hydrogenation of olefins in a solution phase under constant hydrogen pressure.[6a,19] The activity of catalysts can be generally described using a term of "turnover frequency (TOF)" and derived from the slope of the plot. The calculation details are provided under "Characterization" in the Experimental Section and Figure S6. As presented in the inset of Figure 4, Pt_3Fe CNCbs exhibited catalytic activity with a 21.5% enhancement of TOF relative of the cubic counterparts, indicating that the high-index facets are ideal crystal

planes for this surface-sensitive reaction. For liquid-phase hydrogenation, the turnover rate is closely associated with the dissociative adsorption of H_2 and activation of unsaturated bond. Compared to {100} facets, high-indexed planes on the Pt_3Fe CNCbs possess a higher portion of low-coordinated atoms with a unique reactivity which has been demonstrated to cleave H–H and activate C=C bonds more readily.[20] The 10 nm nanocube TOF comparison between the Pt_3Fe and Pt indicates that the hydrogenation of styrene is also sensitive to the composition of catalysts, and incorporation of Fe to Pt NCs leads to an improved catalytic activity. It is well-known that the electronic structure of bimetallic surfaces is distinct from that of the parent metals, resulting in the alteration of surface d-band center and binding strength of adsorbates[21] This modified surface electronic property has been demonstrated to be beneficial to facilitating the hydrogenation of olefins, especially for the Pt-based bimetallic catalysts.[22] In addition, an obvious size effect on the catalytic efficiency of Pt_3Fe CNCbs was revealed. For example, the 10 nm CNCbs were more active than the 20 nm ones. As expected, the decreased size will give rise to a higher surface to volume ratio and percentage of surface atoms, which contributes more to promoting the catalysis. The reusability test was also conducted by using the same Pt_3Fe CNCbs separated from previous reaction system. After consecutively catalyzing this hydrogenation for 24 h, the Pt_3Fe CNCbs were still able to achieve 88% conversion of substrate. No apparent shape difference was observed from the TEM characterization (Figure S5d) when comparing with freshly prepared Pt_3Fe CNCbs, showing high sustainability and recyclability of these Pt_3Fe nanocatalysts in the hydrogenation of styrene.

In addition to the excellent performance in organic hydrogenation, the 10 nm Pt_3Fe CNCbs also exhibit superior catalytic activity toward aqueous-phase reduction of 4-NP by $NaBH_4$ at room temperature. Not merely being a benchmark for testing catalytic activities, it is also a meaningful way to convert more toxic 4-NP to less harmful 4-aminophenol (4-AP) that is a useful intermediate in many drug manufacture.[23] It was reported that the reduction of aromatic nitro compounds by $NaBH_4$ is sensitive to the surface area, structure and composition of the NCs applied as the catalysts.[24] To this end, the effects from the size, shape and introduction of the second metal on the kinetics of this catalytic reaction were assessed by employing 10 nm Pt_3Fe CNCbs as well as 20 nm Pt_3Fe CNCbs, 10 nm Pt_3Fe nanocubes, and 10 nm Pt nanocubes as the counterparts. Considering the color changes involved in this process, Ultraviolet/visible (UV/Vis) spectroscopy was used to monitor the reaction progress, and a kinetic analysis was performed as well. The specific procedures are explicitly described in the Experimental Section. Upon addition of $NaBH_4$, an absorption maximum at 400 nm was detected in the UV/Vis spectrum owing to the formation of 4-nitrophenolate ions in alkaline solution, as shown in Figure 5. The absorbance maintained unchanged at 400 nm in the blank test, revealing that the presence of catalysts was essential for promoting this reaction. After the as-prepared Pt_3Fe CNCb suspensions in ethanol were injected, time-resolved UV/Vis spectra indicate a successive decrease in the absorption band at 400 nm and concomitant emergence of a new peak at 300 nm corresponding to the formation of the product (4-AP). The negligible absorbance at 400 nm indicated a nearly complete conversion of 4-NP after 2700 s, suggesting a high effectiveness of the Pt_3Fe CNCbs as a new class of catalysts.

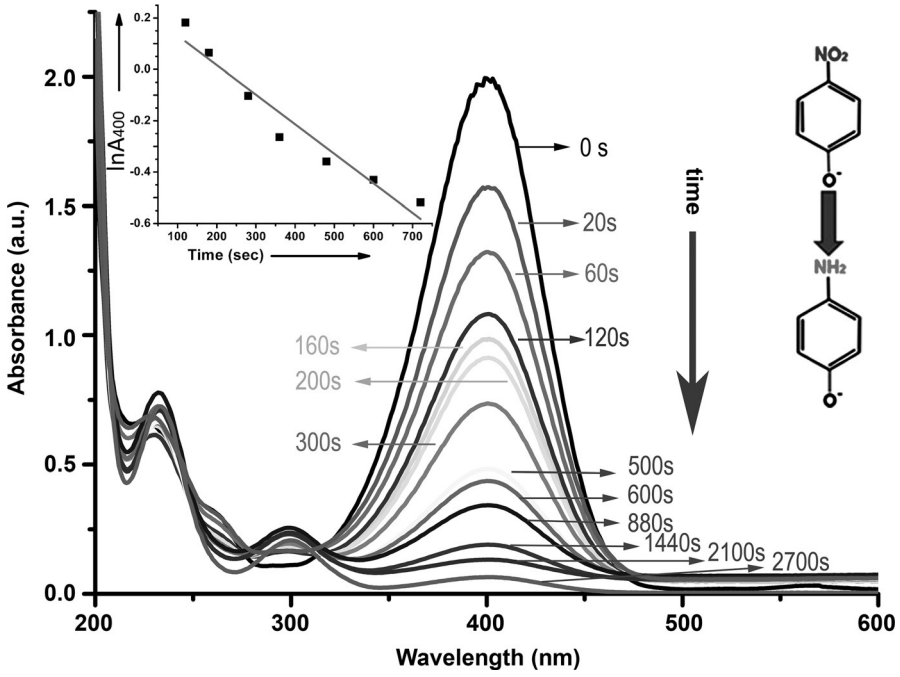

Figure 5. Time-resolved UV/Vis absorption spectra of the reduction of 4-NP by $NaBH_4$ in the presence of 10 nm Pt_3Fe CNCbs. The inset shows a linear relationship between the logarithm of the peak absorbance at 400 nm and reduction time with rate constant obtained from the slope.

As shown in the conversion–time plot (Figure S7a), the reaction rate was fast and steady at the beginning stage and gradually slowed down when most of the reactants were consumed at the end of reduction process. Since the concentration of $NaBH_4$ greatly exceeded that of 4-NP, it can be assumed as a constant during the initial reduction of 4-NP. Therefore, the reaction was considered to follow a (pseudo-) first-order kinetics with respect to 4-NP and the apparent rate constant (k) can be obtained from the first several points in Figure S7a with a plot of $\ln A_{400}$ (A_{400} represents the absorbance at

400 nm) versus time. In this way, the 10 nm Pt_3Fe CNCbs exhibit the highest catalytic activity with an enhanced reaction rate of $k = 1.42 \times 10^{-1}$ min^{-1} (Figure 5), in comparison with those of 10 nm Pt_3Fe nanocubes and 20 nm Pt_3Fe CNCbs by factors of 2.05 and 2.56, respectively (Figure S7 b and c). The 10 nm Pt nanocubes displayed the slowest reduction rate, and the conversion is still far from completion at the 2700 s (Figure S7 d). This outstanding catalytic reactivity on 10 nm Pt_3Fe CNCbs could be ascribed to the common effect of largely accessible active interface sites, higher number of NCs per unit volume, and synergy with heteroatoms on the surface. It is well recognized that the reduction of nitrophenols by $NaBH_4$ involves sequential adsorption steps of nitrophenolate and BH_4^- species to the surface of metallic catalysts and interfacial electron transfer from BH_4^- to nitrophenolate.[24b,25] The concave regions and loosely stacked HIFs on the Pt_3Fe CNCbs provided more available open surfaces for accommodating molecular adsorbates. Meanwhile, an abundance of coordinatively unsaturated atoms were present on the HIFs, acting as suitable catalytic sites with higher reactivity compared to the low-index surface atoms prevalent on nanocubes. The decrease in particle size merited NCs with higher total surface area per unit volume and higher chances of molecular collisions, which is beneficial for the electron transferring process. Moreover, the Fe heteroatoms on the outer layers of Pt_3Fe NCs would function as a catalysis-enhancing agent accounted from the surface electronic property and segregation of the materials on the alloy.

Conclusions

In summary, Pt_3Fe CNCbs terminated with HIFs and a combination of sub-facets {*hk*0} have been developed using a wet-chemical approach. The volume ratio between OAm and OA, capability of the reducing agent, and categories of metal precursors were shown to be key factors to control the particle quality and were subsequently surveyed and optimized. In order to evaluate the surface features, two typical reactions (hydrogenation of styrene and reduction of 4-NP by $NaBH_4$) were studied on this class of HIF nanocatalysts as well as their counterparts in terms of the variations on size, shape, and composition. Results reveal that the 10 nm Pt_3Fe CNCbs exhibited the highest TOF for the hydrogenation of styrene and a promoted reaction rate for 4-NP reduction in comparison with their counterparts. This study provides a new direction for the development of HIF NCs and the exploration of their novel applications serving as enhanced catalysts for useful organic reactions.

Experimental Section

Chemicals

Iron(III) acetylacetonate (99%) was received from STREM Chemicals. Tungsten hexacarbonyl ($W(CO)_6$, 97%), platinum(IV) chloride (98%), sodium borohydride powder (98%), oleic acid (90%), oleylamine (70%) and styrene (99%) were obtained from Sigma–Aldrich. Platinum(II) acetylacetonate (>48% Pt), iron(II) chloride tetrahydrate (98%) and chromium hexacarbonyl ($Cr(CO)_6$, 98%) were purchased from Alfa Aesar. Anhydrous ethanol (200 proof) and anhydrous hexane (98.5%) were produced by AAPER and Fisher Scientific, respectively. Chloroform and d-chloroform (for ^1H NMR) were provided by J.T. Baker and Cambridge Isotope Laboratories, respectively. 4-Nitrophenol (98%, 4-NP) was purchased from ACROS. All chemicals were used without further purification.

Syntheses of Pt_3Fe and Pt NCs

In a typical synthesis of ≈10 nm Pt_3Fe CNCbs, 10.0 mg of iron(III) acetylacetonate ($Fe(acac)_3$), 30.0 mg of platinum(II) acetylacetonate ($Pt(acac)_2$), 10.0 mL of OAm, and 1.0 mL of OA were loaded into a three-neck flask equipped with a condenser and attached to a Schlenk line. The mixture was heated to 140 °C with vigorous stirring under an argon stream. Afterwards, 50 mg of tungsten hexacarbonyl was added into the system, and the temperature was subsequently increased to 240 °C and kept for 40 min with a continuous agitation. The resultant products were isolated by centrifugation, washed with anhydrous ethanol and re-dispersed in hexane for several cycles, and eventually stored in hexane as colloidal suspensions (Figure 1 a). For 20 nm Pt_3Fe CNCb synthesis, the conditions are identical but $W(CO)_6$ was replaced by $Cr(CO)_6$. The conditions for 10 nm Pt_3Fe nanocube synthesis are similar except for replacing $Fe(acac)_3$ with $FeCl_2{\cdot}4H_2O$ and a modification of OAm/OA volume ratio to 8 mL/2 mL. 10 nm Pt nanocubes were synthesized by following the same recipe of Pt_3Fe nanocubes but in the absence of Fe source.

Characterization

Nanocrystal characterization

XRD patterns were collected using a PANalytical X'Pert X-ray powder diffractometer equipped with a $Cu_{K\alpha 1}$ radiation source ($\lambda =$ 1.5406 Å). ICP-OES analysis was carried out on an Optima 7000 DV ICP-OES spectrometer (PerkinElmer). An FEI Tecnai Spirit TEM and 2010F FaStem operated at 120 kV was used for TEM imaging. The HRTEM image was taken from a JEOL TEM 3011. STEM-EDS was performed on Cs-corrected Hitachi2700C with an accelerating voltage of 200 keV. ^1H NMR spectra were recorded on a Bruker AC 300 MHz Proton NMR. UV/Vis spectra were collected at room temperature on a Varian Cary 50 Bio spectrophotometer equipped with a quartz cell.

Catalytic activity evaluation

Hydrogenation of styrene: The synthesized nanocatalysts were cleaned using anhydrous ethanol for several times to remove the capped surfactants. ≈15 mg of each treated NCs were dispersed in 5 mL chloroform with ultrasonication and the suspensions were subsequently transferred into a 10 mL glass reaction vessel. After 0.12 mL of styrene (≈1.00 mmol) was added, an H_2 flow was introduced to blow away the existing air for several minutes. The mixture was kept at room temperature and under 1 atmosphere of H_2 with a high-speed stirring. The collected reaction aliquots were analyzed using ^1H NMR. As shown in Figure S5, feature peaks a, b, c belong to three different olefinic hydrogen atoms in the starting material, whereas the peak d is attributed to the hydrogen atoms on the ethyl group from the product. The conversion of styrene at each specific time is calculated by integrating the area of corresponding peaks. As the ratio between catalysts (mol)/substrate (mol) is 0.023, $TOF = [slope \times 60(min\,h^{-1})]/(0.023 \times 100\%)$, where the slopes are obtained from conversion–time linear relationship in

Figure 4. After the catalysts were cleaned twice using the mentioned procedure, the recycled Pt_3Fe CNCbs (≈15.0 mg) were applied to a reusability test with 1.8 mL of styrene (15 times of the original dosage) and continuous H_2 flow for 24 h, a conversion as high as 88% can still be achieved, implying the desirable stability as catalysts.

Reduction of 4-NP: To investigate the catalytic reduction of 4-NP at room temperature, 14.2 mg (0.1 mmol) of 4-NP was dissolved in 100 mL of de-ionized water through ultrasonication and then 5 mL of ethanol solution containing ≈15 mg nanocatalysts was added under a constant stirring. The original color in dark yellow color quickly turned bright yellow in the mixture, indicating an immediate formation of 4-nitrophenolate (4-NP). Subsequently, 10 mL fresh-made $NaBH_4$ aqueous solution was rapidly injected and the yellowish solution started to fade, indicating the occurrence of reduction. The progress of the conversion of 4-NP to 4-AP was then monitored by recording the time-dependent UV/Vis absorption spectra of the solution in a quartz cuvette sampled from the reaction system. According to lambert-beer's law, the conversion of 4-NP can be calculated as A_t/A_0, where A_t and A_0 represent the absorbance at 400 nm at a specific time and initial time respectively. The rate constants for the pseudo first order reaction under different catalysts can be obtained from the "slope" of the $\ln A_{400}$-t plots in the unit of s^{-1}; $k = (-\text{slope}) \times 60\ \text{sec}\,\text{min}^{-1}$.

Acknowledgements

The authors thank Dr. Jürgen Schulte for his assistance with NMR measurements. Dr. P. Stanley May and Dr. Mary T. Berry at University of South Dakota are gratefully acknowledged for their help in using the TEM facility that was obtained through an NSF grant (CHE-0840507). The HRTEM and STEM/HAADF-STEM-EDS studies were carried out at the Electron Microbeam Analysis Laboratory (University of Michigan) and the Center for Functional Nanomaterials (Brookhaven National Laboratory) which are supported by the US NSF (grant no. DMR-0315633) and the US DOE (contract no. DE-SC0012704), respectively. J.Z. acknowledges the support from the Fundamental Research Funds for the Central Universities (14CX05037A). This work was partially supported by DOE, Analytical and Diagnostics Laboratory (ADL) at Binghamton University.

Keywords: bimetallic nanocrystals · high-index facets · hydrogenation catalysis · shape control · structure dependence

[1] a) L. N. Lewis, *Chem. Rev.* **1993**, *93*, 2693 – 2730; b) N. Chen, W. E. Garwood, F. G. Dwyer, *Shape selective catalysis in industrial applications, Vol. 65*, CRC press, **1996**; c) J. Scherzer, A. J. Gruia, *Hydrocracking science and technology, Vol. 66*, CRC Press, **1996**; d) U. Mueller, M. Schubert, O. Yaghi, G. Ertl, H. Knözinger, F. Schüth, J. Weitkamp, *Handbook of Heterogeneous Catalysis, Vol. 1*, Weinheim, **2008**; e) N. Semagina, L. Kiwi-Minsker, *Catal. Rev.* **2009**, *51*, 147 – 217.

[2] a) Z. L. Wang, *J. Phys. Chem. B* **2000**, *104*, 1153 – 1175; b) A. R. Tao, S. Habas, P. Yang, *Small* **2008**, *4*, 310 – 325; c) Y. Xia, Y. Xiong, B. Lim, S. E. Skrabalak, *Angew. Chem. Int. Ed.* **2009**, *48*, 60 – 103; *Angew. Chem.* **2009**, *121*, 62 – 108.

[3] a) N. Tian, Z. Y. Zhou, S. G. Sun, *J. Phys. Chem. C* **2008**, *112*, 19801 – 19817; b) Z. Y. Zhou, N. Tian, J. T. Li, I. Broadwell, S. G. Sun, *Chem. Soc. Rev.* **2011**, *40*, 4167 – 4185; c) Z. Quan, Y. Wang, J. Fang, *Acc. Chem. Res.* **2012**, *46*, 191 – 202; d) H. Zhang, M. Jin, Y. Xia, *Angew. Chem. Int. Ed.* **2012**, *51*, 7656 – 7673; *Angew. Chem.* **2012**, *124*, 7774 – 7792.

[4] a) S. E. Habas, H. Lee, V. Radmilovic, G. A. Somorjai, P. Yang, *Nat. Mater.* **2007**, *6*, 692 – 697; b) L. Zhang, J. Zhang, Q. Kuang, S. Xie, Z. Jiang, Z. Xie, L. Zheng, *J. Am. Chem. Soc.* **2011**, *133*, 17114 – 17117; c) H. Zhang, M. Jin, J. Wang, W. Li, P. H. Camargo, M. J. Kim, D. Yang, Z. Xie, Y. Xia, *J. Am. Chem. Soc.* **2011**, *133*, 6078 – 6089; d) Y. W. Lee, D. Kim, J. W. Hong, S. W. Kang, S. B. Lee, S. W. Han, *Small* **2013**, *9*, 660 – 665.

[5] a) J. Zhang, H. Yang, J. Fang, S. Zou, *Nano Lett.* **2010**, *10*, 638 – 644; b) J. Wu, A. Gross, H. Yang, *Nano Lett.* **2011**, *11*, 798 – 802; c) J. Zhang, H. Yang, B. Martens, Z. Luo, D. Xu, Y. Wang, S. Zou, J. Fang, *Chem. Sci.* **2012**, *3*, 3302 – 3306; d) C. Cui, L. Gan, H. H. Li, S. H. Yu, M. Heggen, P. Strasser, *Nano Lett.* **2012**, *12*, 5885 – 5889.

[6] a) Y. Wu, S. Cai, D. Wang, W. He, Y. Li, *J. Am. Chem. Soc.* **2012**, *134*, 8975 – 8981; b) Y. Wu, D. Wang, Z. Niu, P. Chen, G. Zhou, Y. Li, *Angew. Chem. Int. Ed.* **2012**, *51*, 12524 – 12528; *Angew. Chem.* **2012**, *124*, 12692 – 12696.

[7] V. R. Stamenkovic, B. Fowler, B. S. Mun, G. Wang, P. N. Ross, C. A. Lucas, N. M. Markovic, *Science* **2007**, *315*, 493 – 497.

[8] B. Lim, Y. Xia, *Angew. Chem. Int. Ed.* **2011**, *50*, 76 – 85; *Angew. Chem.* **2011**, *123*, 78 – 87.

[9] a) J. Wu, J. Zhu, M. Zhou, Y. Hou, S. Gao, *CrystEngComm* **2012**, *14*, 7572 – 7575; b) S. W. Chou, C. L. Zhu, S. Neeleshwar, C. L. Chen, Y. Y. Chen, C. C. Chen, *Chem. Mater.* **2009**, *21*, 4955 – 4961.

[10] J. Zhang, J. Fang, *J. Am. Chem. Soc.* **2009**, *131*, 18543 – 18547.

[11] Y. Yin, A. P. Alivisatos, *Nature* **2005**, *437*, 664 – 670.

[12] B. Lim, X. Lu, M. Jiang, P. H. Camargo, E. C. Cho, E. P. Lee, Y. Xia, *Nano Lett.* **2008**, *8*, 4043 – 4047.

[13] D. Xu, Z. Liu, H. Yang, Q. Liu, J. Zhang, J. Fang, S. Zou, K. Sun, *Angew. Chem. Int. Ed.* **2009**, *48*, 4217 – 4221; *Angew. Chem.* **2009**, *121*, 4281 – 4285.

[14] N. S. Porter, H. Wu, Z. Quan, J. Fang, *Acc. Chem. Res.* **2013**, *46*, 1867 – 1877.

[15] R. Viswanatha, D. D. Sarma in *Nanomaterials Chemistry*, Wiley-VCH, **2007**, pp. 139 – 170.

[16] a) X. Xia, S. Xie, M. Liu, H.-C. Peng, N. Lu, J. Wang, M. J. Kim, Y. Xia, *Proc. Natl. Acad. Sci. USA* **2013**, *110*, 6669 – 6673; b) Z. Quan, W. S. Loc, C. Lin, Z. Luo, K. Yang, Y. Wang, H. Wang, Z. Wang, J. Fang, *Nano Lett.* **2012**, *12*, 4409 – 4413.

[17] a) A. X. Yin, X. Q. Min, W. Zhu, W. C. Liu, Y.-W. Zhang, C. H. Yan, *Chem. Eur. J.* **2012**, *18*, 777 – 782; b) Y. Jiang, Y. Jia, J. Zhang, L. Zhang, H. Huang, Z. Xie, L. Zheng, *Chem. Eur. J.* **2013**, *19*, 3119 – 3124.

[18] a) P. N. Rylander in *Ullmann's Encyclopedia of Industrial Chemistry*, Wiley-VCH, **2000**; b) I. P. Freeman, in *Ullmann's Encyclopedia of Industrial Chemistry*, Wiley-VCH, **2000**.

[19] B. Veisz, Z. Király, L. Tóth, B. Pécz, *Chem. Mater.* **2002**, *14*, 2882 – 2888.

[20] a) G. A. Somorjai, *Chemistry in two dimensions: surfaces, Vol. 290*, Cornell University Press, Ithaca, **1981**; b) S. Schimpf, M. Lucas, C. Mohr, U. Rodemerck, A. Brückner, J. Radnik, H. Hofmeister, P. Claus, *Catal. Today* **2002**, *72*, 63 – 78.

[21] W. Yu, M. D. Porosoff, J. G. Chen, *Chem. Rev.* **2012**, *112*, 5780 – 5817.

[22] Z. Guo, Y. Chen, L. Li, X. Wang, G. L. Haller, Y. Yang, *J. Catal.* **2010**, *276*, 314 – 326.

[23] Y. C. Chang, D. H. Chen, *J. Hazard. Mater.* **2009**, *165*, 664 – 669.

[24] a) C. Y. Chiu, P. J. Chung, K. U. Lao, C. W. Liao, M. H. Huang, *J. Phys. Chem. C* **2012**, *116*, 23757 – 23763; b) S. K. Ghosh, M. Mandal, S. Kundu, S. Nath, T. Pal, *Appl. Catal. A* **2004**, *268*, 61 – 66; c) S. Kundu, K. Wang, H. Liang, *J. Phys. Chem. C* **2009**, *113*, 5157 – 5163.

[25] S. Wunder, F. Polzer, Y. Lu, Y. Mei, M. Ballauff, *J. Phys. Chem. C* **2010**, *114*, 8814 – 8820.

Manuscript received: April 8, 2015
Accepted Article published: May 8, 2015
Final Article published: June 5, 2015